Journal of Pharmaceutical and Biomedical Analysis 119 (2016) 27–36

Contents lists available at ScienceDirect

Journal of Pharmaceutical and Biomedical Analysis

journal homepage: www.elsevier.com/locate/jpba

Clonidine complexation with hydroxypropyl-beta-cyclodextrin: From physico-chemical characterization to *in vivo* adjuvant effect in local anesthesia

Braga M.A.[a], Martini M.F.[b], Pickholz M.[b], Yokaichiya F.[c,d], Franco M.K.D.[c], Cabeça L.F.[e], Guilherme V.A.[a], Silva C.M.G.[a], Limia C.E.G.[a], de Paula E.[a,*]

[a] *Biochemistry and Tissue Biology Department, Biology Institute, State University of Campinas, Campinas, SP, Brazil*
[b] *Faculty of Pharmacy and Biochemistry, University of Buenos Aires, Argentina*
[c] *Nuclear and Energy Research Institute, IPEN–CNEN/SP, Brazil*
[d] *Department of Quantum Phenomena in Novel Materials, Helmholtz-Zentrum, Berlin, Germany*
[e] *Technology Federal University of Parana, Londrina, PR, Brazil*

ARTICLE INFO

Article history:
Received 5 October 2015
Received in revised form
12 November 2015
Accepted 14 November 2015
Available online 18 November 2015

Keywords:
Clonidine
Cyclodextrin
Drug delivery
Magnetic resonance
Molecular dynamics

ABSTRACT

Clonidine (CND), an alpha-2-adrenergic agonist, is used as an adjuvant with local anesthetics. In this work, we describe the preparation and characterization of an inclusion complex of clonidine in hydroxypropyl-beta-cyclodextrin (HP-β-CD), as revealed by experimental (UV–vis absorption, SEM, X-ray diffraction, DOSY- and ROESY-NMR) and theoretical (molecular dynamics) approaches. CND was found to bind to HP-β-CD (K_a = 20 M^{-1}) in 1:1 stoichiometry. X-ray diffractograms and SEM images provided evidence of inclusion complex formation, which was associated with changes in the diffraction patterns of the pure compounds. NMR experiments revealed changes in the chemical shift of $H3_{HP\text{-}\beta\text{-}CD}$ hydrogens (Δ = 0.026 ppm) that were compatible with the insertion of CND in the hydrophobic cavity of the cyclodextrin. Molecular dynamics simulation with the three CND species that exist at pH 7.4 revealed the formation of intermolecular hydrogen bonds, especially for the neutral imino form of CND, which favored its insertion in the HP-β-CD cavity. *In vitro* assays revealed that complexation retarded drug diffusion without changing the intrinsic toxicity of clonidine, while *in vivo* tests in rats showed enhanced sensory blockade after the administration of 0.15% CND, with the effect decreasing in the order: CND:HP-β-CD + bupivacaine > CND + bupivacaine > bupivacaine > CND:HP-β-CD > clonidine. The findings demonstrated the suitability of the complex for use as a drug delivery system for clinical use in antinociceptive procedures, in association with local anesthetics.

1. Introduction

Clonidine (2-[2,6-dichloroaniline]-2-imidazoline, CND) was first synthesized in the 1960s. It was originally used as nasal decongestant. However, due to its capacity to lower blood pressure, CND has been successfully employed in the treatment of hypertension for over 25 years. Nevertheless, other uses in clinical practice were proposed [1], and CND has attracted new interest in anesthesiology, as an adjuvant for general and regional anesthesia during surgery or in the postoperative period [2–5]. It is well known that CND prolongs the effect of local anesthetics, reducing the dosage required for anesthesia, with minor adverse effects [6–10]. This beneficial action is due to different mechanisms. In addition to its α_2-agonist action (norepinephrine-like in descending inhibitory pathways), CND acts analogously to a local anesthetic, inhibiting and slowing impulse conduction in C fibers [11,12]. CND also elicits vasoconstriction, mediated by the postsynaptic α_2-receptors, which reduces absorption of the local anesthetic and prolongs its residence time at the neural tissue [6,7]. In summary, the association of clonidine with local anesthetics significantly reduces the time of onset of anesthesia, prolongs the duration and intensity of the sensory block, and leads to sedation due to systemic absorption [13].

Remko et al. [14], using quantum chemical calculations, found that at the CND equilibrium geometry, the imidazole and phenyl rings of the molecule are almost perpendicular to each other, and

* Corresponding author at: Department of Biochemistry and Tissue Biology, Institute of Biology, State University of Campinas, Rua Monteiro Lobato no 255, 13083-862, Campinas, SP, Brazil. Fax: +55 19 35216185.
E-mail addresses: depaula@unicamp.br, eneidapaula@gmail.com (E. de Paula).

http://dx.doi.org/10.1016/j.jpba.2015.11.015
0731-7085/

it was suggested that this non-coplanarity is required for the interaction of CND with adrenergic receptors. In addition, it was shown that the imino tautomer, with an exocyclic double bond, is the most stable isomer. Moreover, the primary sites of protonation were found to be in the imidazole nitrogens ($pK_a = 8.0$), with protonated and neutral (amino and imino) forms being present at physiologic pH [15].

Drug delivery systems can be used to manipulate the properties of drugs and enhance their therapeutic effects. Cyclodextrins are among the most promising carriers for the sustained release of antinociceptive agents [16,17], and hydroxypropyl-beta-cyclodextrin (HP-β-CD) has been approved for parenteral use [18,19]. It is well tolerated in humans and, after intravenous administration, is almost completely eliminated via glomerular filtration [20]. HP-β-CD has been extensively studied as a carrier system for local anesthetics, with advantages such as improved solubility and clinical potency [20–25].

This work proposes the complexation of CND with hydroxypropyl-β-cyclodextrin, in order to improve its clinical efficacy in anesthesia. A broad study was undertaken, with preparation and characterization of the complex, followed by *in vitro* and *in vivo* tests, and molecular dynamics simulation, with highly encouraging results.

2. Experimental

2.1. Reagents and chemicals

Clonidine hydrochloride was donated by Cristália Ind. Farm. Ltda. (Itapira, SP, Brazil). Hydroxypropyl-β-cyclodextrin (Kleptose HP®) was purchased from Roquette Serv. Tech. Lab. (Lestrem, Cedex, France). D_2O was obtained from Sigma. DMEM (Dubelcco's Modified Eagle Medium) was acquired from Nutricell (Campinas, SP, Brazil). Bovine fetal serum, penicillin, and streptomycin were obtained from Cultilab (Campinas, SP, Brazil). All other chemicals used were of analytical grade.

3. Methods

3.1. Preparation of the clonidine:HP-β-CD complex

Preparation of the inclusion complex was performed by mixing equimolar amounts of CND and HP-β-CD in water, followed by 12 h agitation, to achieve complete solubilization. The samples were freeze-dried and stored at −20 °C for further use.

3.2. UV-Vis absorption study and stoichiometry determination

The interaction between CND and HP-β-CD was followed by UV absorption in the range 250–310 nm. A titration approach was used to determine the complexation stoichiometry [26], with CND spectra recorded in the presence of increasing HP-β-CD concentrations (CND:HP-β-CD molar ratios of 1:0, 1:1, 1:10, 1:20, 1:30, 1:40, 1:50, 1:75, and 1:100). Using the Job plot approach [27], CND spectra were recorded for different CND:HP-β-CD ratios, maintaining a final concentration of CND + HP-β-CD = 2 mM. All experiments were performed in 5 mM Hepes buffer, at pH 7.4 and 25 °C.

The Benesi–Hildebrand procedure was employed to distinguish between the 1:1 and 1:2 stoichiometries, according to [28]:

$$\frac{[\mathrm{CND}]}{\mathrm{Abs} - \mathrm{Abs}_0} = \frac{1}{[\mathrm{HP-\beta-CD}]^n} \quad (1)$$

where [CND] and [HP-β-CD] are the concentrations of CND and HP-β-CD, respectively. Abs (Abs_0) represents the CND absorbance at 271 nm, in the presence (absence) of HP-β-CD, and "*n*" is the stoichiometry of complexation. For the 1:1 stoichiometry, the CND:HP-β-CD association constant (K_a) was calculated from the slope/intercept ratio [28].

3.3. Scanning electron microscopy

Lyophilized samples of the CND:HP-β-CD complex, HP-β-CD, CND, and their physical mixture were deposited on carbon ribbons, previously fixed to aluminum stubs. The stubs were placed in a carbon evaporator (Med 020Coating System, Bal-Tec) and submitted to 3 cycles (20 s) of carbon emission at 75 A. The materials were analyzed with a JSM 500 LV scanning electron microscope, using secondary electron emission.

3.4. X-ray diffraction experiments

Powder diffractograms for samples of HP-β-CD, clonidine, the physical mixture, and the inclusion complex were obtained using a Rigaku wide angle goniometer, equipped with a Cu K_α radiation source (Philips PW 1743), operated at 40 kV and 20 mA. The crystal analyzer was pyrolytic graphite. A scan rate of 1°/min was used, between $2\theta = 5°$ and 60° in a θ–2θ configuration.

3.5. Nuclear magnetic resonance

NMR analyses were performed with a Varian Inova 500 MHz (11.75 T) instrument, at the Brazilian Synchrotron Light Laboratory (LNBio, Campinas, Brazil). One- and two-dimensional ^{1}H NMR spectra were acquired at 25 °C, using D_2O as solvent. Samples (10 mM) of CND, HP-β-CD and the complex were prepared in D_2O at pH 7.4 (adjusted with NaOD and DCl solutions), homogenized for 6 h, and transferred to 5 mm tubes for spectrum acquisition. To avoid any possible interaction with HP-β-CD, no external standards were used [29]; instead, the residual water peak (4.68 ppm) was used as an internal reference.

2D-ROESY experiments were carried out to determine nuclear Overhauser effects (NOE), indicating the spatial proximity between CND and HP-β-CD hydrogens. Rotating-frame cross-relaxations were carried out using spin-locked conditions and NOE in the transverse positive plane. Pulse sequence was employed, with a mixing time of 300 ms [30].

DOSY-NMR spectra were recorded at 25 °C, using the DgcteSL (gradient compensated stimulated echo spin lock) HR-DOSY sequence, as described previously [31]. The amplitudes of the pulsed gradient range were 0.12–0.63 T m^{-1}, where an approximately 90–95% decrease in the resonance intensity was achieved at the largest gradient. For all experiments, 25 different gradient amplitudes were used, with an optimized diffusion time of 0.06 s. The processing program (DOSY macro) was run with data transformed using fn = 32 K.

From the measured diffusion constants (D), the fraction of CND bound to HP-β-CD (f) was determined, according to Eq. (2):

$$f = \frac{D_{\mathrm{CND}} - D_{\mathrm{CND:HP-\beta-CD}}}{D_{\mathrm{CND}} - D_{\mathrm{HP-\beta-CD}}} \quad (2)$$

allowing for the determination of the association constant (K_a), as follows [31]:

$$K_a = \frac{f}{(1-f)([\mathrm{HP-\beta-CD}] - f[\mathrm{CND}])} \quad (3)$$

3.6. Molecular dynamics simulation

Molecular dynamics simulations of the different systems were performed in order to shed light on the interaction between CND and HP-β-CD at the atomic level. Since CND has a pK_a of 8.0 [32],

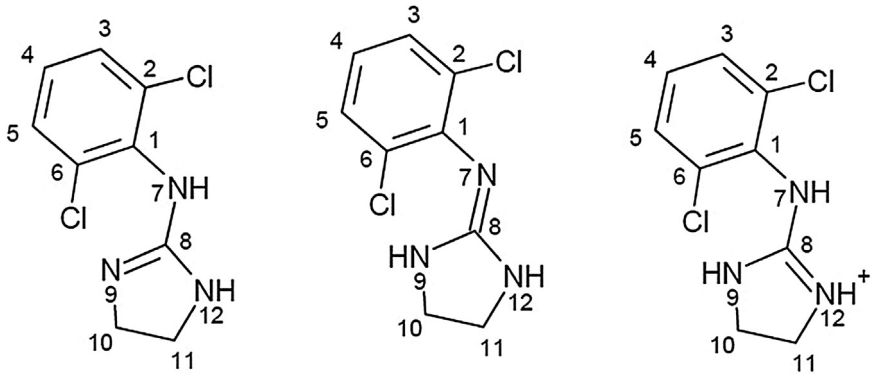

Fig. 1. Three forms of clonidine: (A) amine-imidazoline, (B) imino-imidazoline and (C) protonated.

Table 1
Scheme of selected atoms from the clonidine molecule and their corresponding atomic charge (see Fig. 1 for assignment).

	Amino	Imino	Protonated
N9	−0.476	−0.633	−0.847
H9	0.460	0.324	0.438
N12	−0.150	−0.584	−0.831
H12	–	0.490	0.446
N7	−0.642	−0.915	−0.879
H7	0.378	–	0.446
C8	−0.384	0.780	1.145
C1	−0.708	0.715	0.240

80% of the molecules are found in the protonated state at physiological pH, while 20% are neutral. In its protonated form, the positive charge is shared through resonance by all three nitrogens of the guanidine group. On the other hand, the uncharged CND form presents two tautomeric isomers: amino and imino imidazolidine [33,14], with the imino form being predominant [14]. The three CND forms are shown in Fig. 1. They have a bulky *ortho* chlorine group that prevents the two rings adopting a coplanar conformation [14,15].

In order to carry out the simulations, CND:HP-β-CD complexes with 1:1 stoichiometry were constructed using eight representative relative orientations for each of the forms, surrounded by water molecules. Simulations were performed using the GROMACS 4.5 software package [34–37]. The GROMOS-96 53a6 force field [38] was used for the CND and HP-β-CD molecules. The hydrogen atoms bonded to carbon atoms were treated as the united atoms type. Water was modeled using the simple point charge (SPC) model [39]. Equilibrium bond distances, angles, and dihedrals were obtained from the ground state geometry optimization of the three CND forms, using density functional theory (DFT) with the B3LYP [40] functional and the 6-311G** basis set. The partial atomic charges were obtained from a single point HF/6-31G* calculation, using Gaussian Frisch et al. [41] and Singh and Kollman [42] protocols. The charges of the selected atoms are given in Table 1.

The simulations were carried out within the NVT ensemble, using the Berendsen thermostat [43]. The electrostatic interactions were handled with the SPME version of the Ewald sums [44,45]. The settings for the SPME method were a real space cut-off of 1.4 nm, a grid spacing of 0.12 nm, and a cubic interpolation. In all the simulations, the van der Waals interactions were cut off at 1.4 nm. The whole system was coupled to a controlled-temperature bath, with a reference temperature of 300 K, and the relaxation constant was 0.1 ps. No constraints were used for the bonds. The time step for the integration of the equation of motion was 1 fs. The non-bonded list was updated every 10 steps.

3.7. In vitro dialysis experiments

Drug diffusion experiments experiments were conducted using a two-compartment dialysis system, with a MWCO 1000 Da cellulose membrane (Spectrapore) separating the donor (1 mL) compartment, containing CND or CND:HP-β-CD, from the acceptor compartment (100 mL), containing 20 mM HEPES buffer at pH 7.4, under constant stirring at 37 °C. Aliquots were withdrawn from the acceptor compartment at regular intervals, and the CND concentration was determined at 271 nm.

3.8. Cytotoxicity tests

Perpetual Balb/c mouse fibroblasts (3T3 cells) were routinely grown in DMEM medium containing 10% fetal bovine serum, 100 U/mL penicillin, and 100 μg/mL streptomycin, at 37 °C in a humidified incubator with 5% CO_2. The cells (2×10^4 per well) were incubated in 96-well plates until semi-confluence, followed by treatment for 2 h with CND (free or complexed with HP-β-CD) at concentrations from 0 to 10 mM. After treatment, the cell medium was replaced by a solution of MTT (1 mg/mL) and the cells were incubated for 1 h at 37 °C. Subsequently, the MTT solution was removed and 0.1 mL of pure ethanol was added to dissolve the formazan crystals. The formazan absorbance was measured at 570 nm using a microplate reader (ELx800, BioTek Instruments Inc., USA). The results (mean ± SD) were expressed as percentages of the values obtained for untreated controls [46]. IC_{50} values were determined by nonlinear regression analysis using a sigmoid concentration-response equation obtained for individual experiments, performed with Origin 6.0 (Microcal™ Software Inc., Northampton, MA).

3.9. In vivo analgesia tests

The sensory block was measured by threshold animal tail removal due to a thermal stimulus (the *tail-flick* test) [47]. Six groups of animals (7 male Wistar rats, 250–350 g each) were tested using 20 μL intrathecal administration of cyclodextrin (control), 0.25% BVC, 0.15% CND, 0.15% CND:HP-β-CD, 0.25% BVC + 0.15% CND, and 0.25% BVC + 0.15% CND:HP-β-CD. After injection, the animals were placed in containers with the tail positioned on a heat source and the time for tail removal was measured, as described previously [47]. The protocols were approved by the University of Campinas Institutional Animal Care and Use Committee (protocol 2708-1/2012), following the recommendations of the Guide for the Care and Use of Laboratory Animals.

3.10. Statistical analysis

The release kinetics results were analyzed by means of the two-tailed unpaired *t*-test. The pharmacological data (*in vitro* and *in vivo*) were analyzed by one-way analysis of variance for individual times (with the Tukey–Kramer post-hoc test), using GraphPad Instat (GraphPad Software, Inc., La Jolla, CA, USA) or Origin 6.0 software.

4. Results

4.1. Clonidine UV–vis absorption properties and complexation

The hyperchromic effect obtained after CND complexation was evaluated by measurements of the UV absorption spectra for several CND:HP-β-CD ratios (Fig. 2A and B). The changes in the absorption properties were used to identify complexation [48,49]. Treatment the spectral shifts by the Benesi–Hildebrand approach [28] permitted to identify the prevalence of 1:1 or 1:2CND:HP-β-CD complexation stoichiometry (Fig. 2C and D).

In agreement with the Job plot analysis (Fig. 2A), the linear correlation ($r^2 = 0.9986$) obtained with the Benesi-Hildebrand treatment (Fig. 2D) confirmed the 1:1 complexation stoichiometry. Moreover, the ratio between the slope and intercept of Fig. 3C allowed determination of the binding constant (K_a) of CND to HP-β-CD: 25 M^{-1}. The small K_a value indicates that the forces responsible for maintenance of the complex were small [50].

4.2. Scanning electron microscopy analysis

Fig. 3 shows SEM images of HP-β-CD, CND, the CND:HP-β-CD physical mixture, and the inclusion complex. To exclude any possible influence of the freeze-drying treatment in the morphology, all samples were submitted to lyophilization, prior to SEM analysis. The solid CND sample consisted of hexagonal crystals up to 100 μm in size, with the ternary symmetry that is characteristic of this type of crystal. HP-β-CD consisted of amorphous structures ~50 μm in size. The crystalline and amorphous structures of the pure compounds (CND and HP-β-CD) were preserved in the physical mixture, indicating that complexation did not occur when the solid host and guest compounds were simply mixed together. The CND:HP-β-CD complex presented a poorly defined structure with no resemblance to the HP-β-CD amorphous structure and complete loss of the crystal structure of CND. These morphological alterations provided evidence of inclusion complex formation.

4.3. X-ray diffraction

X-ray diffraction is a useful tool for the qualitative analysis of complexation, by observation of the fingerprints associated with the sample components [51]. The diffractogram for clonidine (Fig. 4D) clearly revealed its crystalline nature, while HP-β-CD was amorphous (Fig. 4A). The diffractogram for the physical mixture of clonidine and HP-β-CD (Fig. 4C) resembled a superpositioning of the crystalline clonidine and the amorphous HP-β-CD patterns. In agreement with the SEM results, the crystalline clonidine pattern was not detected in the inclusion complex diffractogram (Fig. 4B), where the amorphous structure was indicative of the insertion of CND into the cyclodextrin macrocyclic cavity [52]. Furthermore, a 67% decrease in the intensity for the inclusion complex, relative to that of pure HP-β-CD (Fig. 4B *vs.* 4A) was recorded in the 2θ region, revealing a reduction in the HP-β-CD crystallinity.

Table 2
Chemical shift ($\Delta\delta$, ppm) and assignments for CND, in the absence and presence of HP-β-CD.

HP-β-CD	Hydrogen	$\delta_{absence}$	$\delta_{presence}$	$\Delta\delta$
	H_1	4.974	4.966	−0.008
	H_2	3.542	3.535	−0.007
	H_3	3.863	3.837	−0.026
	H_4	3.393	3.390	−0.003
	H_5	3.757	[a]	[a]
	H_6	3.775	3.770	−0.005
	CH_3 (hydroxyl)	1.055	1.049	−0.006
CND	$H_{imidazole}$	3.6806	3.6860	0.0054
	H_{meta}	7.4681	7.4778	0.0097
	H_{meta}	7.4548	7.4642	0.0094
	H_{para}	7.3193	7.3266	0.0073

[a] Not measured because of peak superpositioning.

4.4. Nuclear magnetic resonance

Nuclear magnetic resonance is one of the most powerful tools used to obtain information about inclusion complexes present in solution [53]. Table 2 shows changes in the chemical shifts of the hydrogens of CND and HP-β-CD, in solution and in the presence of each other (CND:HP-β-CD complex), determined at 500 MHz. Assignment of the CND peaks was in agreement with the literature and revealed magnetic equivalent peaks for hydrogens 10 and 11 of the imidazole ring (Fig. 1), at 3.68 ppm, as well as for *meta* hydrogens 3 and 5 (at 7.45 and 7.47 ppm) and *para* hydrogen 4 (at 7.32 ppm) of the phenyl ring. The assignment of hydrogens belonging to HP-β-CD (Fig. 5) was also in accordance with the literature [54–57].

Complexation induced subtle ($\Delta\delta < 0.05$ ppm) non-significant changes in all of the CND hydrogens (Table 2). In the case of the cyclodextrin hydrogens, it was expected that when complexation occurred, hydrogens 3 (H3) and 5 (H5), located in the cavity of the macrocyclic ring of the cyclodextrin, would be influenced by the inclusion of the guest molecule in the cavity [22,56,58]. In the case of the CND:HP-β-CD complex, a slight change ($\Delta\delta = 0.02$ ppm) was observed for the H3 signal (Table 2), while the chemical shift of H5 could not be satisfactorily determined, due to superpositioning with CND peaks.

Nuclear overhauser effect (NOE) [30,59,60] experiments (ROESY) were used to discriminate between the possible modes of encapsulation and provide information on the intermolecular proximity between the hydrogens of the guest molecule included in the HP-β-CD cavity and hydrogens H3 and H5 [59]. No NOE cross-peaks were observed for the aromatic CND hydrogens and H3, but peak overlaps in the 3-4 ppm region (affecting imidazole hydrogens of CND and H5 of HP-β-CD) hindered the analysis.

The lack of interaction between the aromatic CND ring and the HP-β-CD cavity can be explained by the hindrance (steric and polarity) generated by the bulky chlorine atoms substituted in the *ortho* position in the phenyl ring. As found for the imidazole ring, molecular dynamics simulations (see below) revealed that only the interaction of the imino form (representing the minority uncharged CND species at pH 7.4) with the CD cavity was favored.

The use of diffusion (DOSY) experiments is another interesting NMR approach able to provide information about host-guest inclusion complex formation. The diffusion coefficient of a small molecule such as CND is large and decreases with complex formation, which enables DOSY determination of the guest fraction associated with the CD, together with the binding constant (K_a) [61,62]. Here, the DOSY spectrum indicated that the mobility of CND was only slightly decreased after complexation (with diffusion coefficients of 6.20×10^{-10} m^2 s^{-1} and 5.68×10^{-10} m^2 s^{-1} for free and complexed CND, respectively), showing that only 14% of

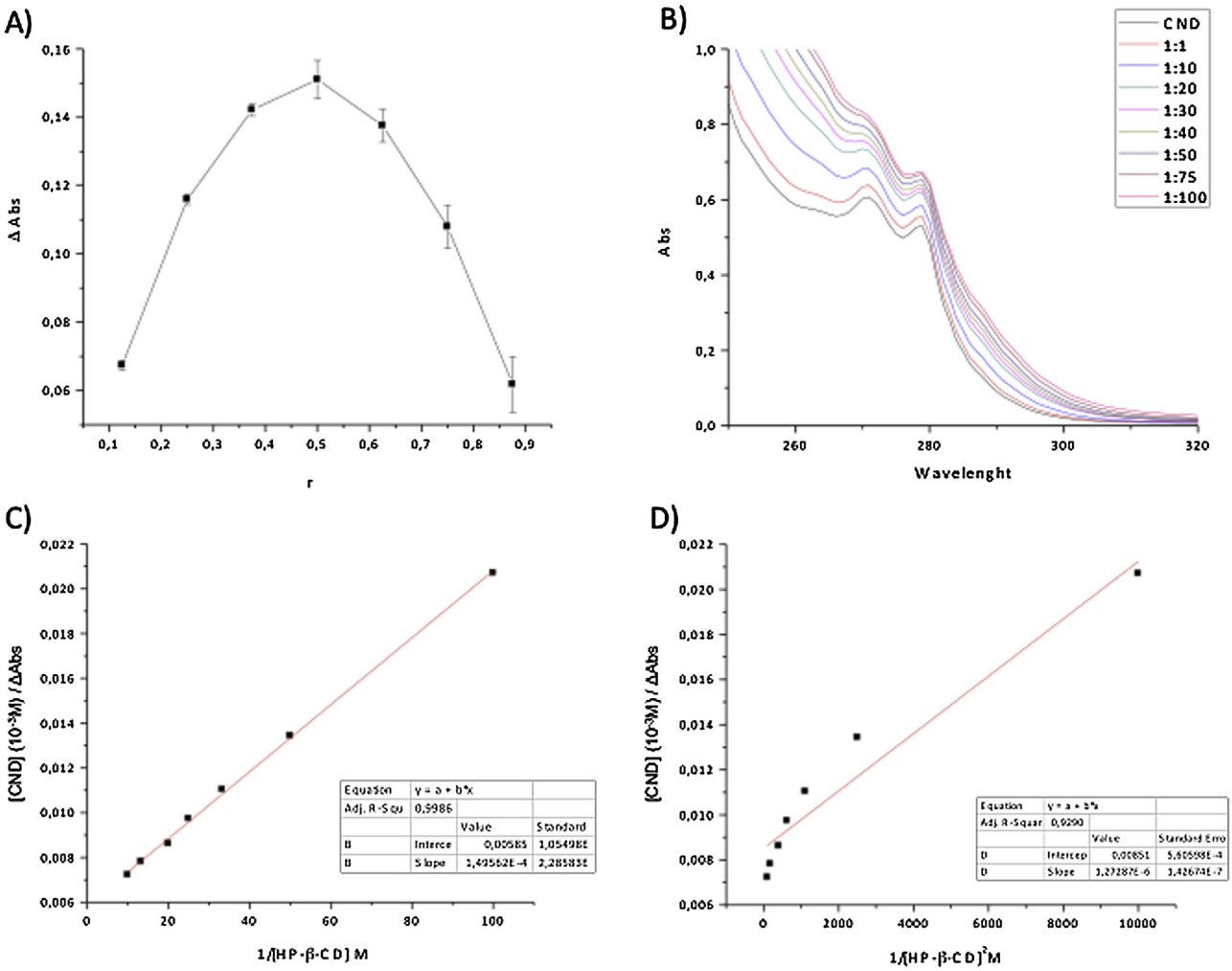

Fig. 2. Clonidine absorption properties in the absence and presence of increasing HP-β-CD concentrations (A) Job plot; (B) spectra for stoichiometry of complexation calculations. (C,D) Benesi–Hildebrand treatments to determine the 1:1CND:HP-β-CD (C) or 1:2CND:HP-β-CD (D).

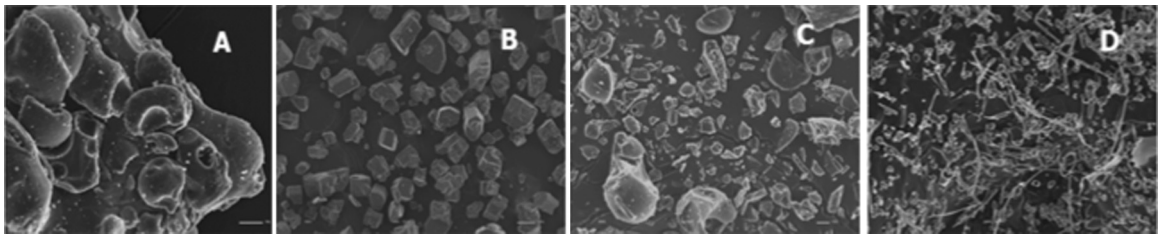

Fig. 3. SEM micrographies of: (A) HP-β-CD (1000×); (B) CND (100×); (C) CND:HP-β-CD physical mixture (1000×); (D) CND:HP-β-CD complex (1000×).

Table 3
Diffusion coefficients (D) of CND, HP-β-CD and CND:HP-β-CD complex, complex molar fraction and CND:HP-β-CD association constant (K_a), as determined by ^{1}H NMR.

Compound	D (10^{-10} m^2 s^{-1})	Complex molar fraction (%)	K_a (M^{-1})
CND	6.20 ± 0.044	–	–
HP-β-CD	2.47 ± 0.011	–	–
CND:HP-β-CD	5.68 ± 0.023	14	20

the CND interacted with HP-β-CD (Table 3). Moreover, the low value of the binding constant (K_a = 20 M^{-1}) is in agreement with that determined with the Benesi–Hildebrand approach (Fig. 2C).

In summary, the NMR results (slight chemical shift changes and small binding constant) were consistent with the formation of a weakly associated inclusion complex, but did not help to identify the part of the CND molecule that was inserted in the HP-β-CD cavity. Further insights into the topology of the complex were therefore obtained using molecular dynamics simulations.

4.5. Molecular dynamics simulations

As already discussed, clonidine can be found in its neutral and protonated forms at pH 7.4. In addition, CND has two tautomeric forms for its neutral state: amino and imino species, with the latter being more stable [14,15]. In this work, the interactions of these three forms with HP-β-CD were investigated. In each case, eight representative pairs (CND-HP-β-CD) were constructed in order to explore the possible relative orientations. The twenty-four pairs

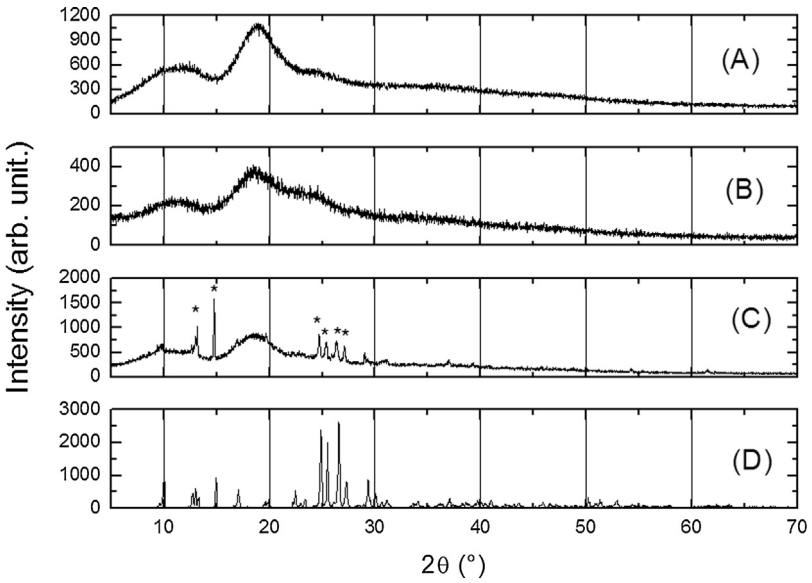

Fig. 4. X-ray diffractograms for: HP-β-CD (A); CND: HP-β-CD complex (B), CND:HP-β-CD physical mixture (C) and CND (D).

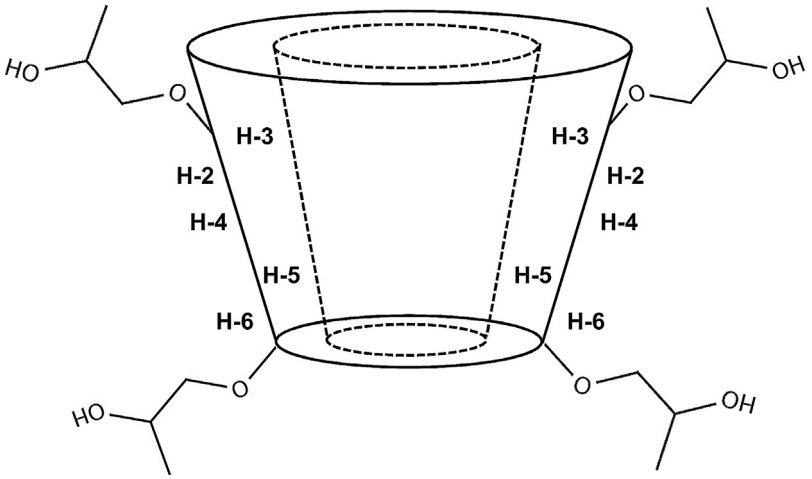

Fig. 5. Schematic representation of an HP-β-CD molecule, showing the assignment of hydrogens from the glucopiranose units. The arrows indicate hydroxypropyl atoms involved in hydrogen bonds (see text).

were simulated up to 100 ns. In order to obtain an initial picture of the behavior of the pairs, calculation was made of the center of mass distances (d_{CMS}) between CND and HP-β-CD. Observation of the temporal evolution of d_{CMS} indicated that only a few of the CND-HP-β-CD pairs remained associated for at least 10 ns during the simulation run. Therefore, it was only considered that association took place when the following criteria were obeyed: d_{CMS} <9 Å, variation of d_{CMS} <3 Å, and maintenance of the complex for ≥10 ns. For those pairs that were found to remain associated for ≥10 ns, Fig. 6 shows the temporal evolution of d_{CMS} and the energy of interaction (E_{int}, in kJ/mol) between CND and HP-β-CD, calculated as the sum of the energies associated with the electrostatic and van der Waals interactions.

For the neutral amino case, only two pairs remained associated for ~20 ns (Fig. 6A). However, they separated and no new complexes were formed during the simulation run, confirming the low complexation affinity of the neutral amino CND form.

On the other hand, in the imino (also neutral) case, four initial configurations led to complexation (Fig. 6B). Notably, the black and red curves show complexes that remained stable over 40 ns (black line) and the total time (100 ns, red line) of the simulation run. For this last case, a schematic diagram of the complex is given in Fig. 7A, showing the formation of two hydrogen bonds, involving the imidazole group of CND (N7 and N12) and atoms outside the cavity (OH and ether oxygen of the hydroxypropyl group; see Figure 5) at the outer perimeter of HP-β-CD. Fig. 7B shows the temporal evolution of the hydrogen bonds for the three nitrogens of a given imino CND:HP-β-CD complex.

The features of the protonated case were intermediate between the other two cases (Fig. 6). In all the cases where complexation was found, investigation was made of the interactions that provided stabilization.

In order to clarify these results, calculation was made of the occurrence of hydrogen bonds between each of the nitrogenous groups (N or NH) of CND and all the potential donors (D) and acceptors (A) of HP-β-CD. The criteria used for hydrogen bond formation was a D-A cut-off distance of 3.1 Å and an H-D-A angle cut-off of 30°. It was concluded from the simulations that complex formation between CND and HP-β-CD depended on the CND form and the initial conditions, as follows:

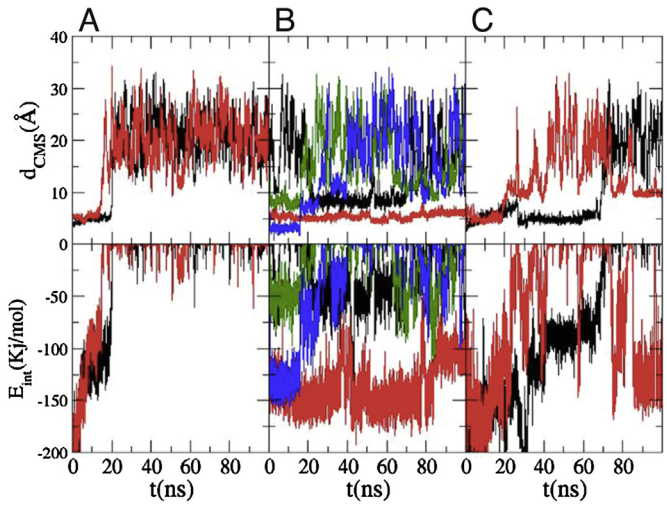

Fig. 6. Molecular dynamic simulations: center-of-mass (d_{CMS}) distance and interaction energies as a function of time for the amino (A), imino (B) and protonated (C) forms of CND. Just the complexes that remained associated for more than 20 ns are shown here.

- CND amino form: hydrogen bond formation was sporadic, even for the two pairs that remained associated over 20 ns of the simulation.
- CND imino form: complex stabilization was stronger than for the amino form. The longer-lasting complex, which remained stable over the entire simulation, was essentially stabilized by the formation of hydrogen bonds, as illustrated in Fig. 7, which shows the number of hydrogen bonds formed as a function of time for N9H, N12H, and N7. The average hydrogen bond formation was quite high: 0.1 for N9H, 0.83 for N12H, and 0.76 for N7. A similar pattern of hydrogen bond formation was detected for the complex corresponding to the green curve in Fig. 6B, despite being weaker and less stable (for only 20 ns) than the complex corresponding to the red curve. The two other pairs that formed complexes (with longer d_{CMS} distances and higher energies; Fig. 6B) were not stabilized by hydrogen bonds.
- CND protonated form: the two complexes shown in Fig. 6C presented hydrogen bond stabilization during the first 19 and 35 ns of the simulation. These complexes therefore remained stable beyond the lifetime of the hydrogen bonds, suggesting a slow hydration process.

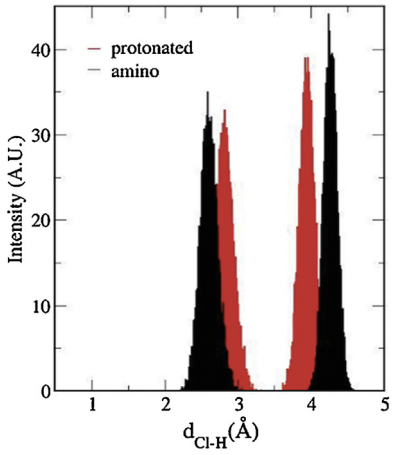

Fig. 8. Histograms of chlorine–hydrogen distances for two selected cases corresponding to amino (in black) and protonated forms of CND.

The results of the simulations suggested that when a complex was formed, the imidazole ring was able to enter the cyclodextrin cavity (especially in the imino case, as discussed below), while entry of the aromatic ring into the cavity was prevented by the presence of chlorine-containing groups.

It is known that chlorine atoms can form weak hydrogen bonds of the O—H···Cl—C type, with a typical distance of 2–3 Å [63,64], although this kind of interaction is uncommon and mainly occurs in intramolecular situations [62]. Here, the protonated and amino CND forms could interact in this way. Analysis was made of the distances between H7 (see Fig. 1), which is only present in these two forms, and each chlorine atom. The results showed that the distance to one of the chlorines was always in the range described for weak hydrogen bonds. A representative example of each of these cases (considering the protonated and amino forms) is shown in Fig. 8, where two well-defined peaks can be observed. This kind of interaction increases the steric hindrance for entry of the molecule into the HP-β-CD cavity and reduces the availability of H3 atoms for formation of intermolecular hydrogen bonds.

In conclusion, the molecular dynamics results showed that the imino form presented the highest capacity for association with HP-β-CD. However, the protonated form is the prevailing species at pH 7.4, which explains the low association constant determined experimentally.

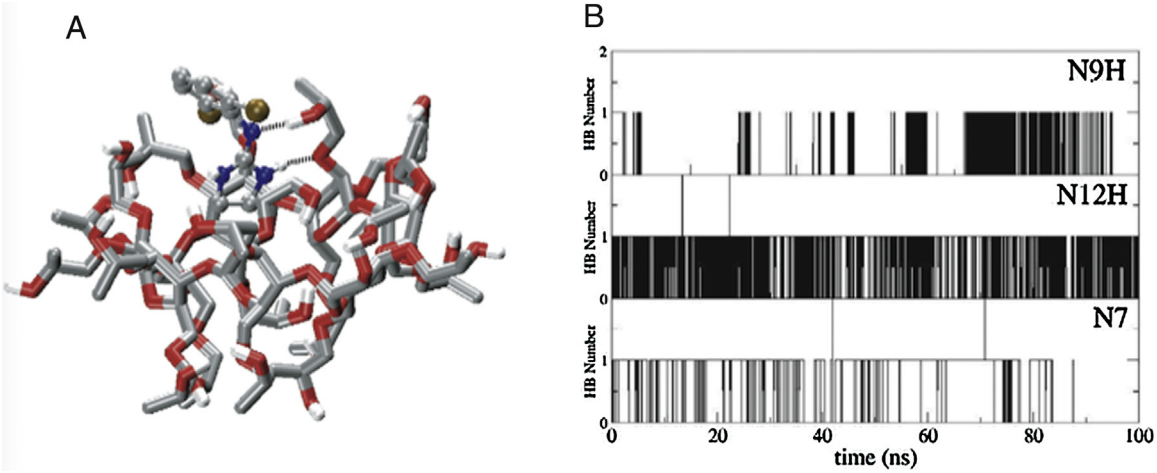

Fig. 7. (A) Snapshot of an inclusion complex between the imine CND form and HP-β-CD, stabilized by hydrogen bonds; (B) number of hydrogen bonds as a function of time for the three nitrogens of a given imino CND:HP-β-CD complex.

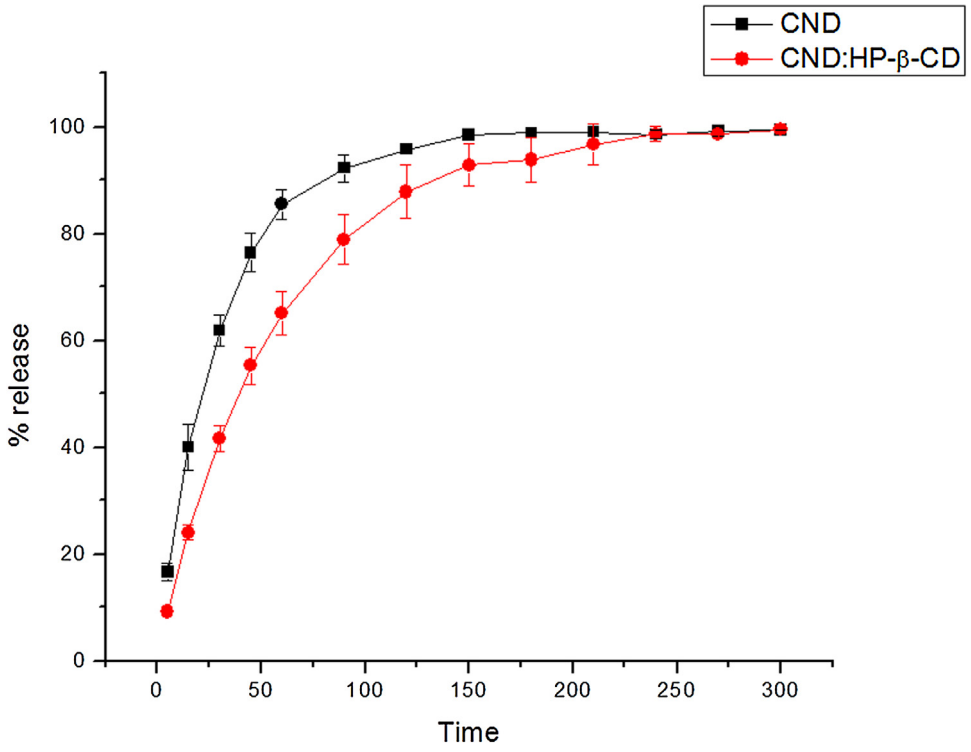

Fig. 9. Dialysis experiments for CND and CND:HP-β-CD in Hepes buffer, pH 7.4, at 25 °C.

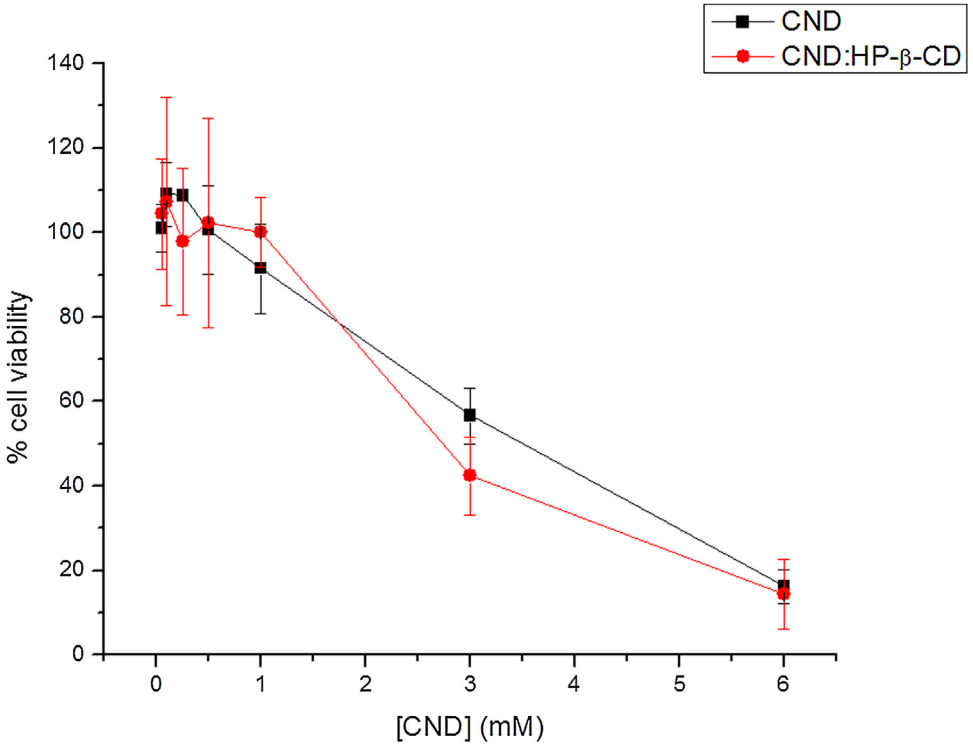

Fig. 10. Cytotoxicity assays showing the survival of 3T3 cells treated for 24 h with CND or CND:β-CD (1:1 molar ratio). The insert shows detail of the 0–1 mM concentration range. MTT reduction test; data presented as percentage of control ($n = 6$).

4.6. Dialysis experiments

It is known that the diffusion rate of drugs can be altered due to complexation. The diffusion of CND complexed to HP-β-CD through polycarbonate membranes was compared to that of the free drug in Hepes buffer at pH 7.4, and followed up to 300 min, when the curves reached equilibrium (Fig. 9). Almost 90% of the free CND was released from the donor compartment after 60 min, compared to 60% of the complexed CND. Although the difference was not pronounced, which may have reflected the low affinity of CND:HP-

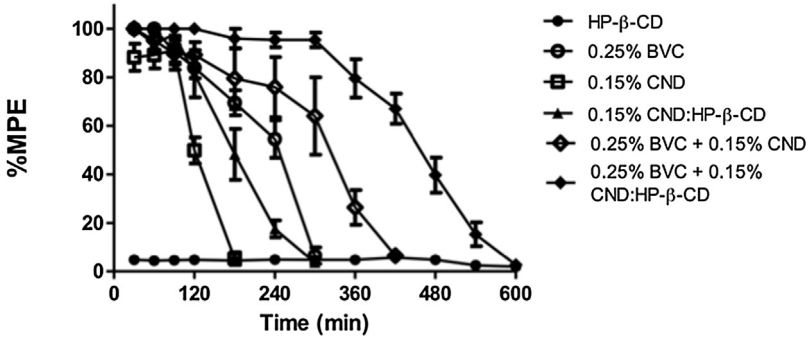

Fig. 11. Sensorial blockage test in Wistar rats after intrathecal administration of 0.15% clonidine (free or HP-β-CD-complexed), 0.25 % bupivacaine (BVC) and their association (BVC + CND and BVC + CND:HP-β-CD). MPE% refers to the percent-anesthetized animals as a function of time ($n = 7$).

β-CD, it was nevertheless significant (AUC values of 25,541.4 ± 21.7 for CND and 24,175.3 ± 38.8 for CND:HP-β-CD, $p < 0.001$), showing that complexation diminished diffusion rate of CND *in vitro*.

4.7. Cytotoxicity studies

Fig. 10 shows the cell viability curves for 3T3 fibroblasts after treatment with free or complexed CND. The IC_{50} values determined for CND and CND:HP-β-CD (3.5 and 2.8 mM, respectively) were not significantly different ($p > 0.05$, Tukey's test). HP-β-CD was not found to be cytotoxic, as shown previously [53]. Hence, from the toxicity point of view, complexation did not change the intrinsic effect of clonidine, which is an important consideration in terms of its safe disposal.

4.8. Analgesia tests

Antinociceptive tests showed that intrathecal administration of 0.15% (20 μL) CND, which was below the concentration that induces hypotension (100 μg) [7], caused sensory blockade of the caudal nerve of rats during 120 min (Fig. 11). Complexation with HP-β-CD significantly prolonged the duration of anesthesia induced by clonidine (180 min, $p < 0.001$, Tukey's test). When associated with 0.25% bupivacaine, this CND concentration prolonged the anesthetic effect to 300 min ($p < 0.01$, Tukey's test), in agreement with previous reports [3–9]. Finally, the combined effect of the CND:HP-β-CD complex and bupivacaine resulted in the extension of anesthesia for as long as 540 min ($p < 0.001$, Tukey's test). These findings reinforced the potential for clinical application of the CND:HP-β-CD complex in surgical procedures, in association with local anesthetics.

5. Conclusions

A CND:HP-β-CD host-guest complex with 1:1 stoichiometry was prepared. XRD and SEM analyses provided evidence of complex formation, as shown by the loss of the crystalline structures of the pure compounds (CND and HP-β-CD). NMR experiments revealed that in solution, the constant for binding of CND to HP-β-CD was low (20 M^{-1}), although it was not possible to obtain molecular details concerning the topology of the complex, due to peak superpositioning. Molecular dynamics simulations confirmed the experimental results, with identification of the formation of stable (that remained through the simulation time) inclusion complexes, notably for the neutral imino form of CND that was stabilized by hydrogen bonding with the cyclodextrin.

In relation to possible applications of the complex as a pharmaceutical drug delivery system, dialysis experiments revealed that complexation slowed the CND diffusion through polycarbonate membranes by 15–20%, while *in vitro* tests revealed that the formation of CND:HP-β-CD did not alter the toxicity profile of CND against fibroblast cells in culture. Antinociceptive studies conducted *in vivo* confirmed that complexation increased the adjuvant effect of clonidine when used together with bupivacaine, a local anesthetic employed in surgical procedures worldwide. Overall, the results obtained in this work support the combined use of the CND:HP-β-CD delivery system and bupivacaine as a novel approach to enhance anesthesia in surgical procedures.

Acknowledgements

Financial support was provided by FAPESP (grant #2006/00121-9) and CNPq (fellowship awarded to E.P.). Clonidine was kindly donated by Cristália Prod. Quim. Farmac. Ltda.

References

[1] M.P.B. Simonetti, E.A. Valinetti, F.M.C. Ferreira, Clonidine: from nasal decongestive to potent analgesic: hystorical and pharmacological considerations, Rev. Bras. Anestesiol. 47 (1997) 37–47.
[2] S. Armand, A. Langlade, A. Boutros, K. Lobjoit, C. Monrigal, R. Ramboatiana, A. Rauss, F. Bonnet, Meta-analysis of the efficacy of extradural clonidine to relieve postoperative pain: an impossible task, Br. J. Anaesth. 81 (1998) 126–134.
[3] C.J.L. MacCartney, E. Duggan, E. Apatu, Should we add clonidine to local anesthetic for peripheral nerve blockade? a qualitative systematic review of the literature, Reg. Anesth. Pain Med. 32 (2007) 330–338.
[4] N. Elia, X. Culebras, C. Mazza, E. Schiffer, M.R. Tramèr, D. Phil, Clonidine as an adjuvant to intrathecal local anesthetics for surgery: systematic review of randomized trials, Reg. Anesth. Pain Med. 33 (2008) 159–167.
[5] D.M. Pöpping, N. Elia, E. Marret, M. Wenk, M.R. Tramer, Clonidine as an adjuvant to local anesthetics for peripheral nerve and plexus blocks: a meta-analysis of randomized trials, Anesthesiology 111 (2009) 406–415.
[6] K. Rhee, K. Kang, J. Kim, Y. Jeon, Intravenous clonidine prolongs bupivacaine spinal anesthesia, Acta Anaesthesiol. Scand. 47 (2003) 1001–1005.
[7] J.F.N.P. Neves, G.A. Monteiro, J.R. Almeida, R.S. Sant'Anna, R.M. Saldanha, E.S. Nogueira, F.L. Coutinho, M.M.P. Neves, F.P. Araújo, P.B. Nobrega, Analgesia pós-operatória para cesariana. A adição de clonidina à morfina subaracnóidea melhora a qualidade da anestesia, Rev. Bras. Anestesiol. 56 (2006) 370–376.
[8] I. Tuijl, W.A. Klei, D.B.M. Werff, C.J. Kalkman, The effect of addition of intrathecal clonidine to hyperbaric bupivacaine on postoperative pain and morphine requirements after caesarian section: a randomized controlled trial, Brit. J. Anesth. 97 (2006) 365–370.
[9] A. Parameswari, A.M. Dhev, M. Vakamudi, Efficacy of clonidine as an adjuvant to bupivacaine for caudal analgesia in children undergoing sub-umbilical surgery, Indian J. Anaesth. 54 (2010) 458–463.
[10] A.F.A. Braga, J.A.F. Frias, F.S.S. Braga, R.I.C. Pereira, S.M.M.C. Titotto, Spinal anesthesia for elective ceasarean section: use of different doses of hyperbaric bupivacaine associated with morphine and clonidine, Acta Cir. Bras. 28 (2013) 26–32.
[11] B. Büttner, B. Ott, R. Klose, Effects of clonidine added to mepivacaine for brachial plexus blockade, Reg. Anesthesiol. 17 (1992) 45.
[12] F.J. Singelyn, M. Dangoisse, S. Bartholomée, Adding clonidine to mepivacaine prolongs the duration of anesthesia and analgesia after axillary brachial plexus block, Reg. Anesthesiol. 17 (1992) 148–150.
[13] J.C. Crews, New developments in epidural anesthesia and analgesia, Anesthesiol. Clin. North Am. 18 (2000) 251–266.
[14] M. Remko, O.A. Walsh, W.G. Richards, Molecular structure and gas-phase reactivity of clonidine and rilmenidine: two layered ONIOM calculations, Phys. Chem. Chem. Phys. 3 (2001) 901–907.

[15] M. Remko, M. Swart, F.M. Bickelhaup, Theoretical study of structure, pK_a, lipophilicity, solubility, absorption, and polar surface area of some centrally acting antihypertensives, Biorgan. Med. Chem. 14 (2006) 1715–1728.
[16] E. de Paula, C.M.S. Cereda, G.R. Tofoli, M. Franz-Montan, L.F. Fraceto, D.R. de Araújo, Drug delivery systems for local anesthetics, Rec. Pat. Drug Deliv. Formul. 4 (2010) 23–34.
[17] E. de Paula, C.M.S. Cereda, L.F. Fraceto, D.R. de Araújo, M. Franz-Montan, G.R. Tofoli, J. Ranali, M.C. Volpato, F.C. Groppo, Micro and nanosystems for delivering local anesthetics, Expert Opin. Drug Deliv. 9 (2012) 1505–1524.
[18] J. Szejtli, Introduction and general overview of cyclodextrin xhemistry, Chem. Rev. 98 (1998) 1743–1753.
[19] M.E. Brewster, T. Loftsson, Cyclodextrin as pharmaceutical solubilizers, Adv. Drug Deliv. Rev. 59 (2007) 645–666.
[20] R. Challa, A. Ahuja, J. Ali, R.K. Khar, Cyclodextrins in drug delivery: an updated review, AAPS Pharm. Sci. Technol. 43 (2005) 329–357.
[21] C. Volobuef, C.M. Moraes, L.A.S. Nunes, C.M.S. Cereda, F. Yokaichiya, M.K.K.D. Franco, A.F.A. Braga, E. de Paula, G.R. Tofoli, L.F. Fraceto, D.R. de Araújo, Sufentanil-2-hydroxypropyl-β-cyclodextrin inclusion complex for pain treatment: physicochemical, cytotoxicity, and pharmacological evaluation, J. Pharm. Sci. 101 (2012) 3698–3707.
[22] L.M.A. Pinto, L.F. Fraceto, M.H.A. Santana, T.A. Pertinhez, S. Oyama Junior, E. de Paula, Physico-chemical characterization of benzocaine-β-cyclodextrin inclusion complexes, J. Pharm. Biomed. Anal. 39 (2005) 956.
[23] C.M. Moraes, P. Abrami, D.R. de Araújo, A.F.A. Braga, M.G. Issa, H.G. Ferraz, E. de Paula, L.F. Fraceto, Characterization of lidocaine:hydroxypropyl-β-cyclodextrin inclusion complex, J. Incl. Phenom. 57 (2007) 313–316.
[24] C.M. Moraes, P. Abrami, E. de Paula, A.F.A. Braga, L.F. Fraceto, Study of the interaction between S(−) bupivacaine and 2-hydroxypropyl-β-cyclodextrin, Int. J. Pharm. 331 (2007) 99–106.
[25] R.A.F. Lima, M.B. de Jesus, C.M.S. Cereda, G.R. Tofoli, L.F. Cabeça, I. Mazzaro, L.F. Fraceto, E. de Paula, Improvement of tetracaine antinociceptive effect by inclusion in cyclodextrins, J. Drug Target. 20 (2012) 85–96.
[26] N.S. Sosnowska, Fluorometric determination of association constants of three estrogens with cyclodextrins, J. Fluoresc. 7 (3) (1997) 195–200.
[27] A.A.A. Shafi, S.S. Shihry, Fluorescence enhancement of 1-napthol-5-sulfonate by forming inclusion complex with β-cyclodextrin in aqueous solution, Spectrochim Acta. 72 (2009) 533–537.
[28] R. Banerjee, H. Chakraborty, M. Sarkar, Host-guest complexation of oxicam NSAIDs with β-cyclodextrin, Biopolymers 75 (2004) 355–365.
[29] Y. Matsui, S. Tokunaga, Internal reference compounds available for the determination of binding constants for cyclodextrin complexes by ^{1}H NMR spectrometry, Bull. Chem. Soc. Jpn. 69 (9) (1996) 2477–2480.
[30] L.F. Cabeça, I.M. Figueiredo, E. de Paula, A.J. Marsaioli, Prilocaine-cyclodextrin-liposome: effect of pH variations on the encapsulation and topology of a ternary complex using ^{1}H NMR, Magn. Reson. Chem. 49 (6) (2011) 295–300.
[31] L.M. Arantes, C. Scarelli, A.J. Marsaioli, E. de Paula, S.A. Fernandes, Proparacaine complexation with β-cyclodextrin and *p*-sulfonic acid calix[6]arene, as evaluated by varied ^{1}H-NMR approaches, Mag. Res. in Chem. 47 (2009) 757–763.
[32] J.E. Thompson, A Practical Guide to Contemporary Pharmacy Practice, 3rd ed., Lippincott Williams and Wilkins, Baltimore, 2009.
[33] T.L. Lemke, D.A. Williams, Foye's Principles of Medicinal Chemistry, 6th ed., Lippincott Williams & Wilkins, Baltimore, 2008.
[34] H.J.C. Berendsen, D. van der Spoel, R. van Drunen, GROMACS: a message-passing parallel molecular dynamics implementation, Comp. Phys. Commun. 91 (1–3) (1995) 43–56.
[35] E. Lindahl, B. Hess, D. van der Spoel, GROMACS 3.0: a package for molecular simulation and trajectory analysis, J. Mol. Model. 8 (2001) 306–317.
[36] D. van Der Spoel, E. Lindahl, B. Hess, G. Groenhof, A.E. Mark, H.J. Berendsen, GROMACS: fast, flexible, and free, J. Comput. Chem. 16 (2005) 1701–1718.
[37] B. Hess, C. Kutzner, D. van der Spoel, E. Lindahl, GROMACS 4: algorithms for highly efficient, load-balanced, and scalable molecular simulation, J. Chem. Theory Comput. 3 (2008) 435–447.
[38] C. Oostenbrink, A. Villa, A.E. Mark, W.F. van Gunsteren, A biomolecular force field based on the free enthalpy of hydration and solvation: the GROMOS force-field parameter sets 53A5 and 53A6, J. Comput. Chem. 13 (2004) 1656–1676.
[39] H.J.C. Berendsen, J.P.M. Postma, W.F. van Gunsteren, J. Hermans, Interaction models for water in relation to protein hydration, in: B. Pullman (Ed.), Intermolecular Forces, Reidel, Dordrecht, 1981, pp. 331–342.
[40] A.D. Becke, Density functional thermochemistry III: the role of exact Exchange, J Chem. Phys. 98 (1993) 5648.
[41] M.J. Frisch, G.W. Trucks, H.B. Schlegel, G.E. Scuseria, M.A. Robb, J.R. Cheeseman, V.G. Zakrzewski, J.J.A. Montgomery, R.E. Stratmann, J.C. Burant, S. Dapprich, J.M. Millam, A.D. Daniels, K.N. Kudin, M.C. Strain, O. Farkas, J. Tomasi, V. Barone, M. Cossi, R. Cammi, B. Mennucci, C. Pomelli, C. Adamo, S. Clifford, J. Ochterski, G.A. Petersson, P.Y. Ayala, Q. Cui, K. Morokuma, D.K. Malick, D. Rabuck, K. Raghavachari, J.B. Foresman, J. Cioslowski, J.V. Ortiz, B.B. Stefanov, G. Liu, A. Liashenko, P. Piskorz, I. Komaromi, R. Gomperts, R.L. Martin, D.J. Fox, T. Keith, M.A. Al-Laham, C.Y. Peng, A. Nanayakkara, C. Gonzalez, M. Challacombe, P.M.W. Gill, B. Johnson, W. Chen, M.W. Wong, J.L. Andres, C. Gonzalez, M. Head-Gordon, E.S. Replogle, J.A. Pople, GAUSSIAN98 (Revision A.7), Gaussian Inc., Pittsburgh, PA, 1998.
[42] U.C. Singh, P.A. Kollman, An approach to computing electrostatic charges for molecules, J. Comput. Chem. 5 (1984) 129.
[43] H.J.C. Berendsen, J.P.M. Postma, W.F. van Gunsteren, A. DiNola, J.R. Haak, Molecular dynamics with coupling to an external bath, J. Chem. Phys. 81 (1984) 3684–3690.
[44] T. Darden, D. York, L. Pedersen, Particle mesh ewald: an Nlog(N) method for Ewald sums in large systems, J. Chem. Phys. 12 (1993) 10089–10092.
[45] U. Essmann, L. Perera, M.L. Berkowitz, T. Darden, H. Lee, L.G. Pedersen, A smooth particle mesh Ewald method, J. Chem. Phys. 19 (1995) 8577–8593.
[46] T. Mosmann, Rapid colorimetric assay for cellular growth and survival: application to proliferation and cytotoxicity assays, J. Immunol. Methods 65 (1983) 55–63.
[47] S.D. Al Sharari, F.I. Carroll, J.M. McIntosh, M.I. Damaj, The antinociceptive effects of nicotinic partial agonists varenicline and sazetidine-A in murine acute and tonic pain models, J. Pharm. Exp. Ther. 342 (2012) 742–749.
[48] W. Misiuk, M. Zalewska, Spectroscopic investigations on the inclusion interaction between hydroxypropyl-β-cyclodextrin and bupropion, J. Mol. Liq. 159 (2011) 220–225.
[49] C. Tablet, I. Matei, M. Hillebrand, The determination of the stoichiometry of cyclodextrin inclusion complexes by spectral methods: possibilities and Limitations, in: Stoichiometry and Research—The Importance of Quantity in Biomedicine, Alessio Innocenti Ed., 2012.
[50] Y.L. Loukas, V. Vraka, G. Gregoriadis, Drugs in cyclodextrins in liposomes: a novel approach to the chemical stability of drugs sensitive to hydrolysis, Int. J. Pharm. 162 (1998) 137–142.
[51] P. Mura, Analytical techniques for characterization of cyclodextrin complexes in solid state: a review, J. Pharm. Biomed. Anal. 113 (2015) 226–238.
[52] D.R. de Araújo, S.S. Tsuneda, C.M.S. Cereda, F.D.G.F. Carvalho, P.S.C. Preté, S.A. Fernandes, F. Yoikaichiya, M.K.K.D. Franco, I. Mazzaro, L.F. Fraceto, A.F.A. Braga, E. de Paula, Development and pharmacological evaluation of ropivacaine-2-hydroxypropyl-β-cyclodextrin inclusion complex, Eur. J. Pharm. Sci. 33 (2008) 60–71.
[53] P. Mura, Analytical techniques for characterization of cyclodextrin complexes in aqueous solution: a review, J. Pharm. Biomed. Anal. 101 (2014) 238–250.
[54] V.V.A. Castelli, G. Trivieri, I. Zucchelli, L. Brambilla, T. Barbuzzi, C.M. Castiglioni. Paci, G. Zerbi, M. Zanol, Characterization of an inclusion complex between cladribine and 2-hydroxypropyl-β-cyclodextrin, J. Pharm. Sci. 97 (2008) 3897–3906.
[55] A.F.V.B. Soares, L.F. Fraceto, E.R. Maia, I.S. Resck, M.J. Kato, E.S. Gil, A.R. Sousa, L.C. Cunha, K.R. Rezende, Host?guest system of 4-nerolidylcatechol in 2-hydroxypropyl-β-cyclodextrin: preparation, characterization and molecular modeling, J. Incl. Phenom. Macrocycl. Chem. 64 (2009) 23–35.
[56] E. de Paula, D.R. de Araújo, L.F. Fraceto, Nuclear magnetic resonance spectroscopy tools for physicochemical characterization of cyclodextrin inclusion, in: Jie Hu (Ed.), Cyclodextrins: Chemistry and Physics, Res. Signpost/Transworld Res. Network, 2010 (Org.) ISBN: 978-81-7895-430-1.
[57] J.Y. Tsao, C.P. Wu, H.H. Tsai, K.C. Peng, P.Y. Lin, S.Y. Su, L.D. Chen, F.J. Tsai, Y. Tsai, Effect of hydroxypropyl-beta-cyclodextrin complexation on the aqueous solubilitystructure, thermal stability, antioxidant activity, and tyrosinase inhibition of paeonol, J. Incl. Phenom. Macrocycl. Chem. 72 (2012) 405–411.
[58] R. Grillo, N.F.S. Melo, L.F. Fraceto, C.L. Brito, H.G. Trossini, C.M.S. Menezes, E.I. Ferreira, C.M. Moraes, Physico-chemical characterization of inclusion complex between hydroxymethylnitrofurazone and hydroxypropyl-beta-α-cyclodextrin, Quim. Nova 31 (2008) 290–295.
[59] H.P. Mo, T.C. Pochapsky, Intermolecular interactions characterized by nuclear Overhauser effects, Prog. Nucl. Magn. Reson. Spectrosc. 30 (1997) 1–38.
[60] A. Chen, M. Shairo, Nuclear Overhauser effect on diffusion measurements, J. Am. Chem. Soc. 121 (1999) 5338–5339.
[61] G.A. Morris, Diffusion-ordered spectroscopy (DOSY), Encycl. Nucl. Magn. Reson. 9 (2002) 35–44.
[62] K.F. Morris, C.S. Johnson, Diffusion-ordered 2-dimensional nuclear-magnetic-resonance spectroscopy, J. Am. Chem. Soc. 114 (8) (1992) 3139–3141.
[63] C.B. Aakeröy, T.A. Evans, K.R. Seddon, I. Pálinkó, The CHCl hydrogen bond: does it exist? New J. Chem. 23 (1999) 145–152.
[64] G.R. Desiraju, T. Steiner, The Weak Hydrogen Bond in Structural Chemistry and Biology, vol. 9, Oxford Univ. Press, UP, Chichester, 1999.